Karlsruhe Institute of Technology

Elektrotechnisches Institut (ETI)
Prof. Dr.-Ing. Michael Braun
Prof. Dr.-Ing. Martin Doppelbauer
Prof. Dr.-Ing. Marc Hiller
Kaiserstr.12. 76131 Karlsruhe

Elektrotechnisches Institut

Title:	Simple Strategy of Overmodulation in Control of Interior Permanent Magnet Synchronous Machines for Improving Efficiency in Automotive Applications
Authors:	Tobias Gemaßmer, Mathias Schnarrenberger, Helmut Späth, Michael Braun
Institute:	Karlsruhe Institute of Technology (KIT) Elektrotechnisches Institut (ETI) Electrical Drives and Power Electronics
Type:	Conference Proceedings
Published at:	PCIM EUROPE 2013 - International Exhibition and Conference for Power Electronics, Intelligent Motion, Renewable Energy and Energy Management Nuremberg, 14-16 May 2013 Publisher: VDE Verlag, Berlin ISBN: 978-3-8007-3505-1 Pages: 231-238
Hyperlinks:	https://www.vde-verlag.de/buecher/563505/pcim-europe-2013.html www.pcim-europe.com

Simple Strategy of Overmodulation in Control of Interior Permanent Magnet Synchronous Machines for Improving Efficiency in Automotive Applications

Tobias Gemaßmer, Mathias Schnarrenberger, Helmut Späth, Michael Braun
Institute of Electrical Engineering (ETI) - Electrical Drives and Power Electronics
Karlsruhe Institute of Technology (KIT), Kaiserstr. 12, 76131 Karlsruhe, Germany
Tel.: +49 721 608 42476, E-mail: tobias.gemassmer@kit.edu

Abstract

In automotive applications, efficiency of the drive train is very important due to the limited energy in the battery. Improvement can be achieved by increasing the inverter output voltage through overmodulation. This can be used for either increasing output power or reducing power losses.

This paper presents a new strategy of voltage limitation for the current control of three-phase electric drives. The proposed limitation scheme allows the use of dynamic rotor-oriented current control with no modifications for operation in overmodulation range. The novel limitation structure is described and verified through simulations and experimental results.

1 Introduction

A simple approach to increase efficiency of torque control of electric machines is to achieve the desired torque with the lowest possible current in order to reduce copper losses. For interior permanent magnet synchronous machines (IPMSM) supplied by voltage source inverters (VSI) this is accomplished by choosing current components for operation with maximum torque per ampere (MTPA) [1]. When reaching higher speed, the voltage exceeds the limit of the inverter, so additional field weakening becomes necessary. In order to keep copper losses low, this should be accomplished by use of the maximum inverter output voltage.

2 Voltage Gain by use of overmodulation

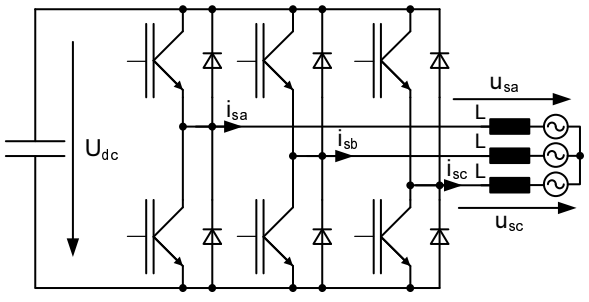

Figure 1: Voltage source inverter

In fig. 2a the region of the possible inverter output voltage vector of a VSI (fig. 1) is shown. It is limited by the shape of a hexagon. To achieve sinusoidal output voltage, the voltage space

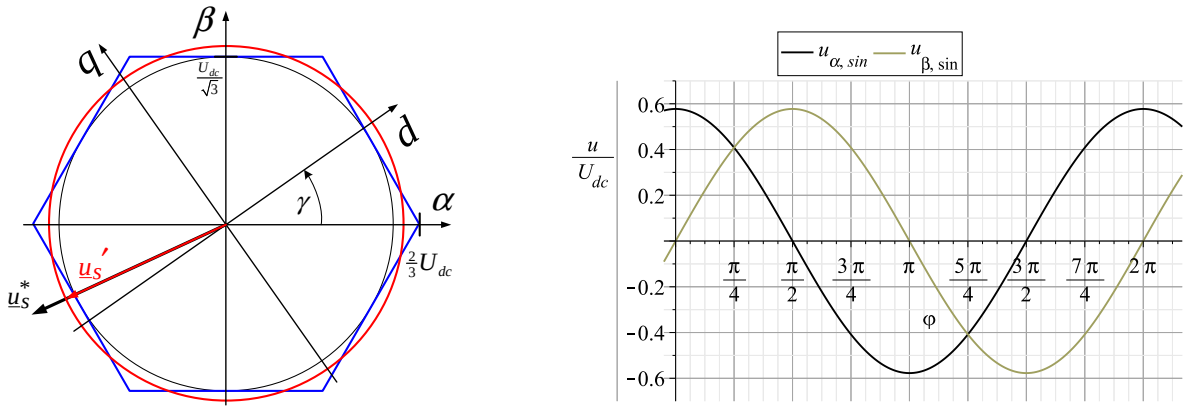

(a) (b)

Figure 2: Trajectory of voltage space vector (a) and voltage components for maximum sinusoidal output voltage (b)

vector is always located inside the inner circle of the hexagon, with a maximum amount of $|\underline{u}_\mathrm{s}| = \frac{U_\mathrm{dc}}{\sqrt{3}}$. The waveforms of the voltage components u_α and u_β for maximum sinusoidal output voltage are shown in fig. 2b.

For the case of overmodulation, the voltage space vector may also be located in the area between the hexagon and the inner circle. The maximum output voltage for the voltage space vector moving with constant angular speed is being reached when moving along the edge of the hexagon. The waveforms of the voltage components for this case are shown in fig. 3a and 3b.

They can be defined piecewise by

$$u_\alpha(\varphi) = \begin{cases} \frac{2}{3+\sqrt{3}\cdot\tan(\varphi)}\cdot U_\mathrm{dc} & \text{if } 0 \le \varphi < \frac{\pi}{3} \\ \frac{\sqrt{3}}{3\cdot\tan(\varphi)}\cdot U_\mathrm{dc} & \text{if } \frac{\pi}{3} \le \varphi < \frac{2\pi}{3} \\ \frac{2}{-3+\sqrt{3}\cdot\tan(\varphi)}\cdot U_\mathrm{dc} & \text{if } \frac{2\pi}{3} \le \varphi < \pi \\ \frac{2}{-3-\sqrt{3}\cdot\tan(\varphi)}\cdot U_\mathrm{dc} & \text{if } \pi \le \varphi < \frac{4\pi}{3} \\ -\frac{\sqrt{3}}{3\cdot\tan(\varphi)}\cdot U_\mathrm{dc} & \text{if } \frac{4\pi}{3} \le \varphi < \frac{5\pi}{3} \\ \frac{2}{3-\sqrt{3}\cdot\tan(\varphi)}\cdot U_\mathrm{dc} & \text{if } \frac{5\pi}{3} \le \varphi < 2\pi \end{cases} \tag{1}$$

and

$$u_\beta(\varphi) = \begin{cases} \frac{2}{\sqrt{3}+\frac{3}{\tan(\varphi)}}\cdot U_\mathrm{dc} & \text{if } 0 \le \varphi < \frac{\pi}{3} \\ \frac{1}{\sqrt{3}}\cdot U_\mathrm{dc} & \text{if } \frac{\pi}{3} \le \varphi < \frac{2\pi}{3} \\ \frac{2}{\sqrt{3}-\frac{3}{\tan(\varphi)}}\cdot U_\mathrm{dc} & \text{if } \frac{2\pi}{3} \le \varphi < \pi \\ \frac{2}{-\sqrt{3}-\frac{3}{\tan(\varphi)}}\cdot U_\mathrm{dc} & \text{if } \pi \le \varphi < \frac{4\pi}{3} \\ -\frac{1}{\sqrt{3}}\cdot U_\mathrm{dc} & \text{if } \frac{4\pi}{3} \le \varphi < \frac{5\pi}{3} \\ \frac{2}{-\sqrt{3}+\frac{3}{\tan(\varphi)}}\cdot U_\mathrm{dc} & \text{if } \frac{5\pi}{3} \le \varphi < 2\pi \end{cases} \tag{2}$$

Fourier analysis of either component u_α or u_β yields the amplitude of the fundamental when moving along the edge of the hexagon to

$$\hat{U}_{\alpha,1} = \hat{U}_{\beta,1} = \frac{\sqrt{3}\cdot\ln 3}{\pi}\cdot U_\mathrm{dc} \tag{3}$$

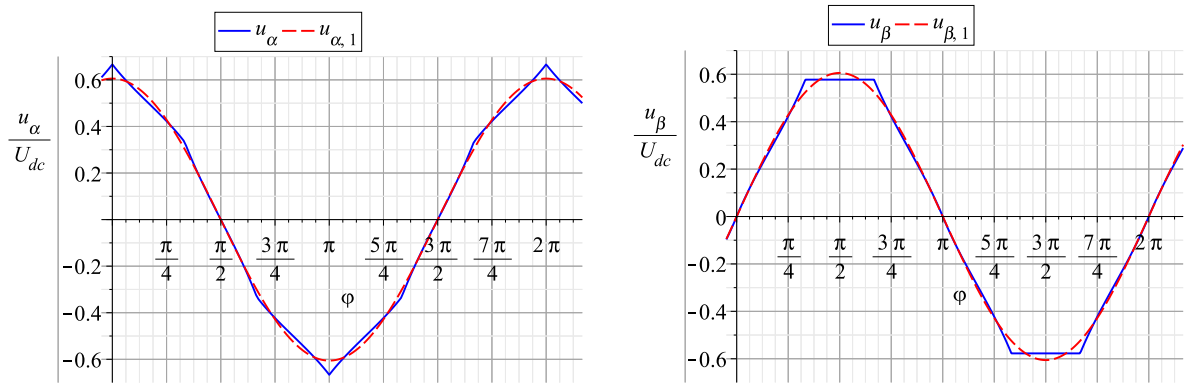

(a) (b)

Figure 3: Waveform of voltage components for maximum output voltage with constant angular speed and the corresponding fundamental

The fundamentals of the voltage components correspond to the dashed red line in fig. 3a resp. 3b. The resulting space vector trajectory for that fundamental voltage describes a circle in the stationary frame presented by the red line in fig. 2a. Compared to sinusoidal output voltage, we have an increase of $\approx 5\ \%$ in voltage fundamental.

Challenges of overmodulation in closed loop current control

However, for dynamic closed loop current control, use of overmodulation brings up two problems [2]:

1. Additional current harmonics are produced due to harmonic output voltages. The current controllers will respond to these harmonics with additional reference voltages.
2. Since the inverter is supposed to operate near its voltage limit in steady-state operation, the demanded voltage will repetitively exceed this limit. This can be seen in fig. 2a: Especially when the voltage space vector is being located close to any of the midpoints of the hexagon's sides, its length exceeds the achievable output voltage. Anti-windup with use of the saturated voltage will prevent the current controller from demanding voltage space vectors near the corners of the hexagon.

Both of these problems are solved by use of the described scheme of limitation.

3 Structure of limitation

Since output torque depends mainly on the current fundamental, the current reference values i_d^* and i_q^* for steady-state operation in field weakening area are calculated for a voltage fundamental of $\left|\underline{u}_{\mathrm{s},1}\right| = \frac{\sqrt{3}\cdot\ln 3}{\pi}\cdot U_\mathrm{dc}$. In the first part of the limitation scheme, "Limitation to fundamental" in fig. 4, the demanded voltage space vector $\underline{u}_\mathrm{s}^* = u_\mathrm{d}^* + j\cdot u_\mathrm{q}^*$ is truncated to that value. At this point, different methods of voltage limitation are possible.The modified voltage components u_d' and u_q' are used for back calculation for anti-windup of the current control.

As can be seen in fig. 5, the relation between the reference space vector $\underline{u}_\mathrm{s}'$ and the resulting fundamental voltage has linear behaviour as long as $|\underline{u}_\mathrm{s}'| \leq \frac{U_\mathrm{dc}}{\sqrt{3}}$. In this case, $\underline{u}_\mathrm{s}'$ lies inside

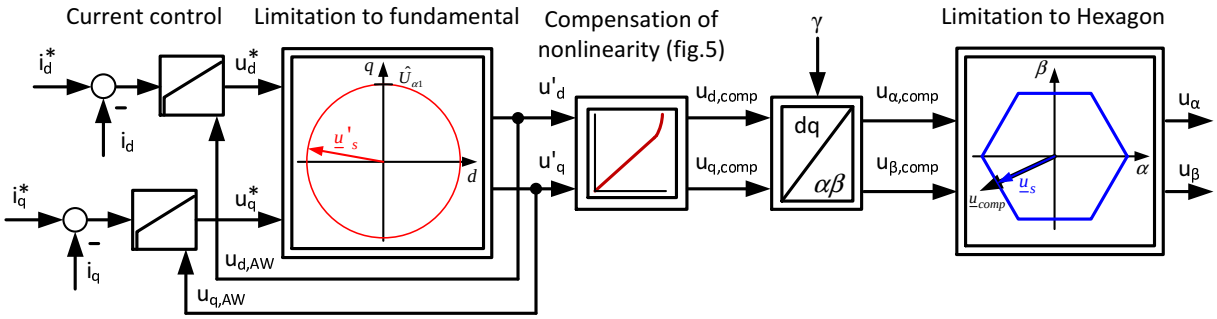

Figure 4: Limitation scheme for overmodulation

the inner circle of the hexagon. For the case $|\underline{u}'_{\mathrm{s}}| > \frac{U_{\mathrm{dc}}}{\sqrt{3}}$, the behaviour becomes nonlinear (see [3]). Fig. 5 shows the characteristics for use of discontinuous pulse width modulation with a continously moving voltage space vector inside of the blue border line in fig. 2a. In order to achieve the desired voltage fundamental, this nonlinearity is compensated by calculation of $\underline{u}_{\mathrm{s,comp}}$.

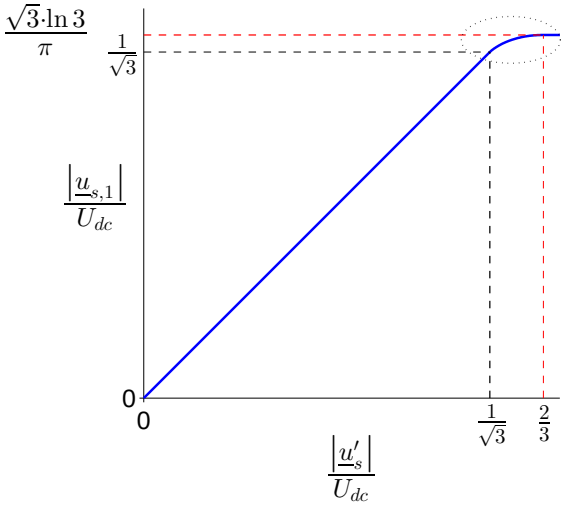

Figure 5: Relation between reference space vector and resulting fundamental voltage.

Since the hexagon is located in the $\alpha\beta$-plane, hexagon limitation should be done after transforming $\underline{u}_{\mathrm{s,comp}}$ back to the stationary frame. In contrary, limitation to fundamental can be done either in stationary or rotating frame. Due to back-calculation for anti-windup of the current controllers, dq-plane might be preferred.

After compensation and coordinate transformation, the voltage space vector $\underline{u}_{\mathrm{s,comp}}$ is limited onto the hexagon without modification of the angle. This is necessary for passing values to the modulator that can actually be reached by the inverter phase legs. The resulting voltage components u_α and u_β can be passed to any kind of modulator that is able to include overmodulation, i.e. space vector modulator or carrier based modulator with injected zero-sequence.

The loop for current control can be closed directly through the measured current components i_{d}, i_{q}, as shown in fig. 4. Neither estimation of current harmonics (see [4]) nor additional inverter model (see [2]) are required.

4 Simulation results

Simulations of the proposed control scheme have been made with an IPMSM designed for electric vehicle with parameters as seen in tab. 1. Current control has been implemented with PI-controllers, designed according to the modulus optimum method [5]. Anti-windup has been accomplished by back-calculation with use of the saturated voltage components u'_{d} and u'_{q}. Results for steady state operation can be seen in fig. 6 and fig. 7.

DC link Voltage	U_{dc}	250 V
Rated current	I_{N}	121 A
Speed	n	5200 min^{-1}
Torque reference	T^*	50 Nm
pole pairs	p	3
Resistance	R_{s}	10 mΩ
Inductance	L_{d}	0.35 mH
Inductance	L_{q}	1.5 mH
PM-Flux linkage	Ψ_{PM}	0.065 Vs

Table 1: Simulation parameters

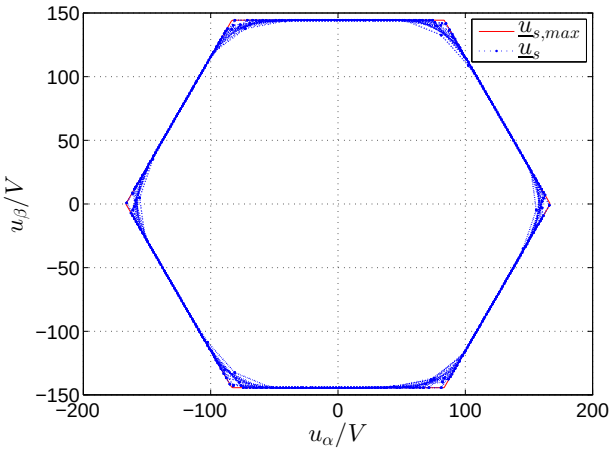

Figure 6: Simulated trajectory of output voltage during overmodulation

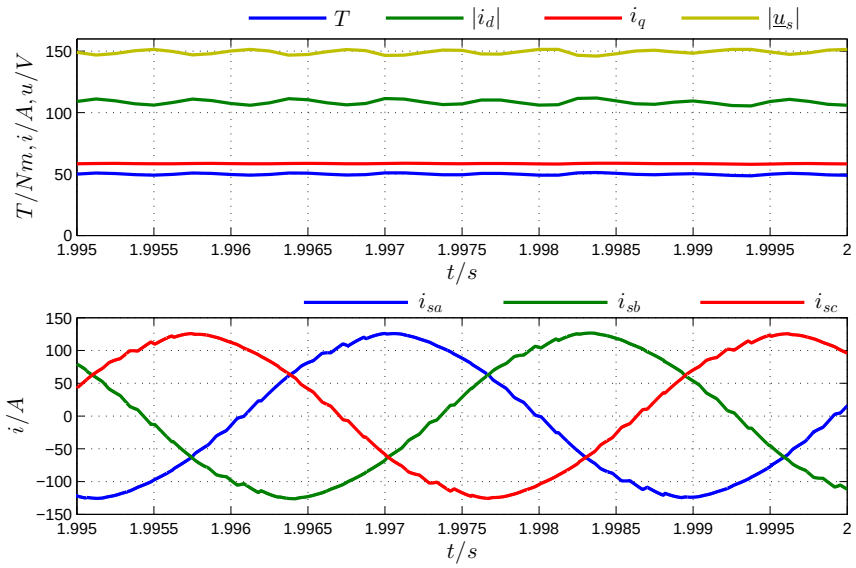

Figure 7: Simulation results

As can be seen in fig. 6, the voltage space vector moves along the outer edge of the hexagon, so complete overmodulation region is reached. The voltage fundamental equals $\frac{\sqrt{3}\cdot \ln 3}{\pi}\cdot U_{\mathrm{dc}}$.

According to fig. 7, the current components show a ripple with a frequency of $f_{\mathrm{har}} = 6 \cdot f_1$ due to overmodulation, which results in a small torque ripple. Because of $L_{\mathrm{d}} < L_{\mathrm{q}}$, the current ripple of component i_{d} is significantly larger than of i_{q}. However, the shape of the phase current is nearly sinusoidal.

5 Experimental results

Measurements on a machine test bench have also been made, using the described limitation scheme for overmodulation. On the test bench current control has been implemented as a state controller based on the design methods of [6].

Fig. 8 shows torque, current components and stator voltage for a speed of $n = 5200\ \mathrm{min}^{-1}$ and a torque reference value of $M^* = 50\ \mathrm{Nm}$, which equals the operating point of the presented simulation results on the previous page. As can be seen, the amount of the stator voltage vector stays mainly constant at $|\underline{u}_\mathrm{s}| = \frac{U_\mathrm{dc}}{\sqrt{3}} \approx 144\ \mathrm{V}$ with sinusoidal output voltage. In contrast, by use of overmodulation, the stator voltage ranges from $|\underline{u}_\mathrm{s}| = \frac{U_\mathrm{dc}}{\sqrt{3}}$ to $\frac{2}{3}U_\mathrm{dc}$.

The impact of the variable stator voltage on the current components is rather small. There is no significant difference between the quality of the current control by use of sinusoidal output voltage or overmodulation. Therefore overmodulation has no influence on the resulting torque.

However, because of the higher stator voltage, the requested torque can be reached with less stator current because less field-weakening is necessary. Therefore, the amount of the current component i_d becomes smaller, i_q becomes slightly higher by use of overmodulation.

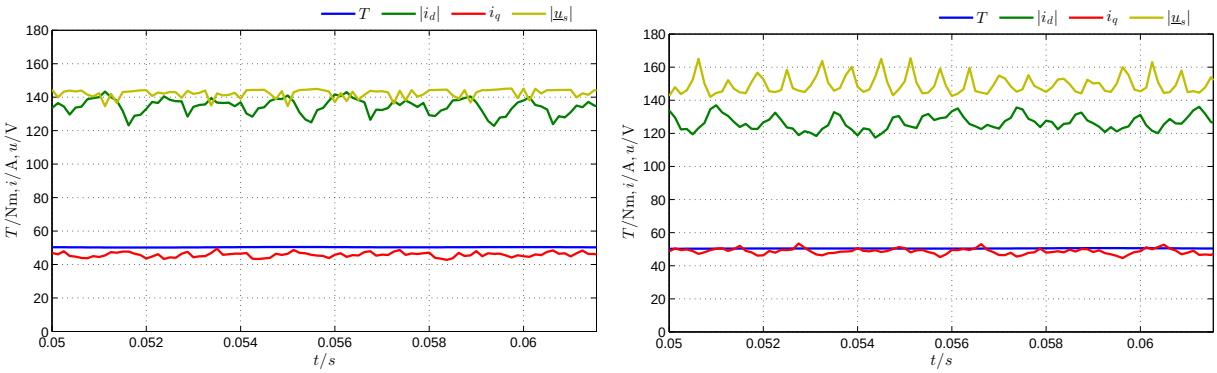

Figure 8: Experimental results: Torque, current components and stator voltage.
(a): Sinusoidal output voltage. (b): Overmodulation.

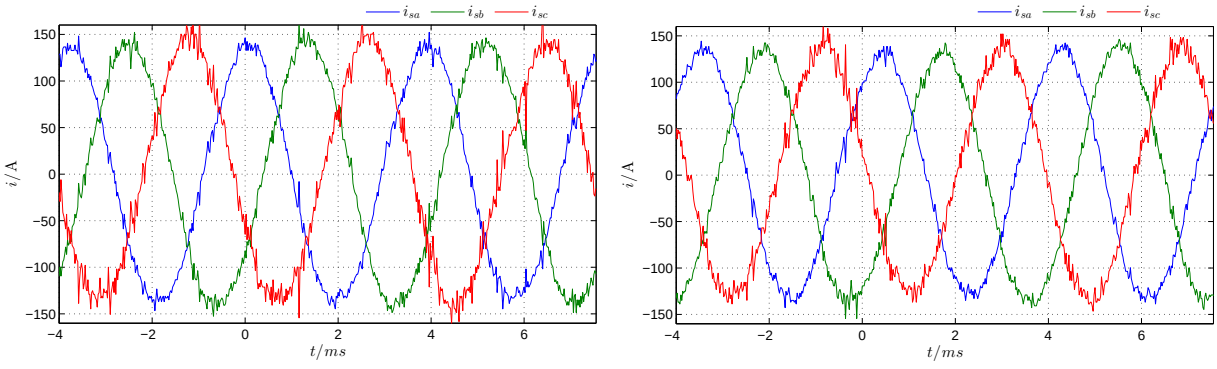

Figure 9: Stator currents. (a): Sinusoidal output voltage. (b): Overmodulation.

	Sinusoidal voltage	Overmodulation
I_{rms}	101.2 A	96.21 A
THD	8.58 %	8.78 %
P_{dc}	30.447 kW	30.192 kW
P_{el}	29.882 kW	29.739 kW
Power Losses VSI	564.9 W	452.3 W
P_{mech}	26.335 kW	26.335 kW
Power Losses IPMSM	3527.4 W	3404.1 W
Total power losses	4092.3 W	3856.4 W

Table 2: Measured powerlosses and harmonics

The described effects can be confirmed regarding the measured phase currents of the IPMSM in fig. 9: The shape of the current is nearly sinusoidal for both sinusoidal output voltage and overmodulation, whereas the amptlitude is slightly smaller while using overmodulation.

Compared to the simulation results, the current values are different in the experimental results, although they represent the same operating point . This is the result of saturation effects within the machine, which have different influences on the inductances L_{d} and L_{q}.

The advantage of the use of overmodulation concerning the power losses can clearly be seen regarding tab. 2, which contains the results of power measurements in the described operation point of the IPMSM with a *Norma D6000*. The decrease of the current rms value for overmodulation is being approved. However, due to the variable amount of the stator voltage, current harmonics increase. This is being indicated by a higher THD, which is being defined as

$$THD = \frac{\sqrt{I_{\mathrm{rms}}^2 - I_1^2}}{I_1} \tag{4}$$

Although higher current harmonics cause additional losses in the machine, the reduction of ohmic losses in both IPMSM and VSI due to the lower current predominates. Therefore the power losses in both IPMSM and VSI decrease through the use of overmodulation. The relative reduction of power losses by changing from sinusoidal output voltage to overmodulation is

$$\Delta P_{\mathrm{rel}} = \frac{4092.3\ \mathrm{W} - 3856.4\ \mathrm{W}}{4092.3\ \mathrm{W}} = 5.8\ \% \tag{5}$$

Verification of the functionality of the proposed limiting scheme can be made by regarding fig. 10a, which shows the trajectory of the voltage space vector $\underline{u}_{\mathrm{s}}$ in the $\alpha\beta$-plane for both sinusoidal output voltage and overmodulation. The trajectory for sinusoidal output voltage has the shape of a circle, whereas use of the proposed limitation scheme associated with the appropriate current reference values causes the output voltage to move along the operating limit of the VSI.

Overmodulation can also be used to increase the maximum power output of the IPMSM. Fig. 10b shows the measured limiting curve of the IPMSM with the rated current of $I_{\mathrm{N}} = 121$ A with and without overmodulation. As long as the speed is lower than $n \approx 3300\ \mathrm{min}^{-1}$, the maximum torque is the same for both operation modes, since the stator voltage stays below the maximum inverter output voltage. For higher speeds, the higher stator voltage at overmodulation allows current component values which result in torque values that are $\approx 5\ \%$ higher than those from sinusoidal output voltage.

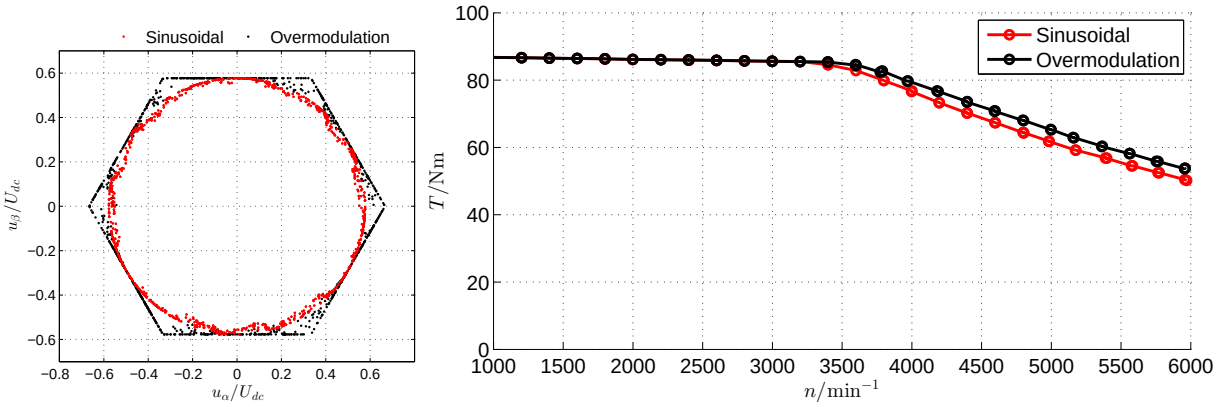

Figure 10: Trajectory of stator voltage space vector (a) and limiting curve of the IPMSM (b)

6 Conclusion

A novel strategy for voltage limitation in a closed-loop current control including overmodulation is introduced, which needs no estimation of current harmonics. Simulation and experimental results show the operation of the novel scheme. A significant decrease of power loss at same power output due to lower current in the machine as well as in the inverter is verified by measurements. An increase in maximum power output has also been demonstrated by experimental results.

References

[1] S. Morimoto, M. Sanada, and Y. Takeda. Wide-speed operation of interior permanent magnet synchronous motors with high-performance current regulator. *Industry Applications, IEEE Transactions on*, 30(4):920 –926, jul/aug 1994.

[2] S. Lerdudomsak, S. Doki, and S. Okuma. A novel current control system for pmsm considering effects from inverter in overmodulation range. In *Power Electronics and Drive Systems, 2007. PEDS '07. 7th International Conference on*, pages 794 –800, nov. 2007.

[3] A.M. Hava, R.J. Kerkman, and T.A. Lipo. Carrier-based pwm-vsi overmodulation strategies: analysis, comparison, and design. *Power Electronics, IEEE Transactions on*, 13(4):674 –689, jul 1998.

[4] A.M. Khambadkone and J. Holtz. Compensated synchronous pi current controller in overmodulation range and six-step operation of space-vector-modulation-based vector-controlled drives. *Industrial Electronics, IEEE Transactions on*, 49(3):574–580, Jun.

[5] Karl J. Åström and T. Hägglund. *PID controllers: theory, design, and tuning*. Instrument Society of America, 2nd edition, 1995.

[6] U. Nuß. *Eine allgemeine Methodik zur Modellbildung und Reglersynthese für stromrichtergepeiste Antriebe auf der Basis der zeitdiskreten Zustandsraumdarstellung*. PhD thesis, Universität Karlsruhe, 1994.